Image analysis, evidence accumulation,
fuzzy methods, histogram, Hough transform

Leszek J. CHMIELEWSKI *

ACCUMULATION METHODS IN THE PROCESSING OF DIFFICULT IMAGES

The accumulation methods emerged in close relation to the development of the Hough transform (HT). The application of some far reaching generalizations of the HT will be presented. The accumulation principle will be taken as a starting point: Accumulate the relevant data from possibly many, possibly competent sources. This principle is known and widely used in image processing, mainly in the methods related to the HT. The principle is in opposition to the tendency to compress the image data as early in the processing as possible. The accumulation principle is a recommendation to utilize the redundancy in the image data in a specific way and should be applied when the images are difficult to process due to their low quality. The basic data structure is the fuzzy histogram, which is in fact an experimentally obtained approximation of the probability density of the phenomenon of interest. The concepts of a degree of fuzzification and the weakly and strongly fuzzified histograms will be introduced. A number of solutions found with the use of the accumulation principle will be presented. In the examples and tests, biomedical images will be used. Such images are challenging because the objects imaged are irregular and the quality of the images is usually limited in a natural way by the imaging modalities used. The accumulation methods are a good solution to the problem of analysis of such images.

1. INTRODUCTION

The image information is scattered. It is a sparse case when for finding an information on a given pixel it is enough to analyse this pixel and its immediate neighbourhood consisting of four or eight pixels. As a rule, it is necessary to analyse either a large neighbourhood of each pixel, or even the whole image.

Let us look at the images in Fig. 1. The problem is to find the edges in a somewhat noisy image of Fig. 1a. The edges shown in the image b were found by analysing the intensities of three pixels for each source pixel, while in the image c the neighbourhood containing about 54 pixels on the average were analysed. The difference in the quality of the results is clearly visible.

Within the domain of image processing, a method in which the data coming from the large parts of the image is *accumulated* in order to obtain the result is the Hough transform in its original form [10, 11] and its numerous derivatives which emerged as an answer to the necessity of detecting complex parametric shapes in difficult cases (see for example [13, 15, 17] for reviews). The fundamental data structure used in the Hough transform is the *accumulator* which has been originally conceived as a table which should capture the *votes* on the specific values of the parameters. This table can be treated as an *experimental probability*

* Institute of Fundamental Technological Research, Polish Academy of Sciences (IPPT PAN). Świętokrzyska 21, PL 00-049 Warsaw, Poland. E-mail: lchmiel@ippt.gov.pl

density of the parameters of the shape to be detected, represented in the quantised parameter space. This representation is in fact a *histogram* of the votes. The *mode* of the histogram (an index for which the histogram has the maximum value) is equivalent to the mode of the probability density function, thus providing an estimate of the measured value. The subset of the set of data from which the parameters constituting one vote is formed is called the *voting subset*. Here, we shall extend the considerations to the detection of non-parametric shapes, so the voting will take place directly in the image space and the accumulator will be compatible with this space. The voting subset will be a selected subset of image pixels.

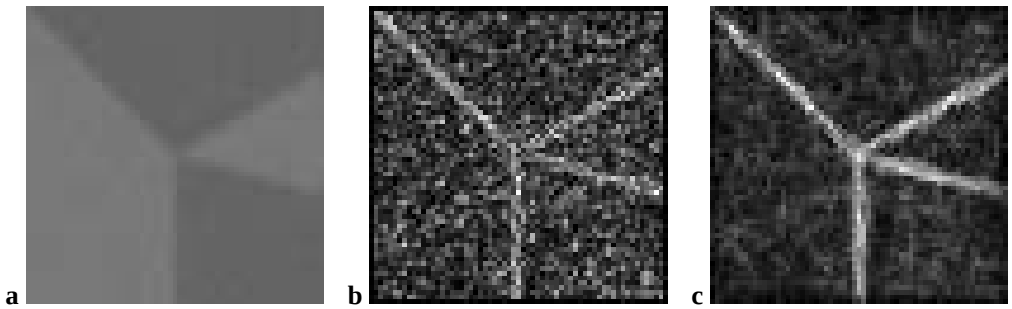

Fig. 1 Example of edge detection. (a) Source image (normal noise, standard deviation = 2); (b) result found using three-pixel neighbourhoods; (c) result found using neighbourhoods containing around 54 pixels on the average

In this paper some results already published in [3, 4, 5, 6] will be presented. Moreover, in Section 3 also those parts of the book [2] which have never been published in English before will be summarised.

2. EVIDENCE ACCUMULATION AND FUZZY HISTOGRAMS

2.1. MEASUREMENTS, ERRORS, OUTLIERS AND INLIERS

Image intensity in a pixel can be treated as a *measurement*, as well as a result of some calculation performed on a number of such intensities, for example, an image gradient. Each measurement will constitute a voting subset. The measurements can be erroneous. Accurate measurements and those with small random errors (such that an average is a good estimate of the correct value) are usually called *inliers*, in opposition to the *outliers*, which can be either the totally incorrect values, called *gross errors*, or the values coming from a phenomenon which is not an original object of interest. Gross errors, if not eliminated, do nothing else than spoiling the result. Values from other phenomena should be properly taken into account provided that these phenomena are important.

An example from the domain of image processing can be the detection of a single bright circle in the dark background. Some bright pixels form the most conspicuous circle: these are the inliers. Others are fragments of other shapes present in the image, or just noise, and these are *outliers*. If any of them is included into the circle sought, it will spoil the result, and this will be a gross error. However, some of the outliers can form another circle, the presence of which was unexpected. A smart detector should warn on the presence of such a case, so that the user or another instance can decide what to do: perhaps the assumption that there is always only a single circle in the image is too simple.

A broad discussion on the inliers and outliers, their types and methods of their treatment with robust statistics can be found in [8]. The methods described here will make only indirect reference to robust statistics. Another domain which is closely related to the considerations presented is the kernel density estimation (see for example [16]). Here we shall stay on the grounds of image processing.

2.2. FUZZY HISTOGRAMS

Let us consider the following example of $K = 20$ measurements $\bar{x}^k, k = 1,...,K$, shown schematically in Fig. 2. One measurement is one voting subset. It can be noted that the majority of the measurements appear in the interval $\langle 14.5, 17.5 \rangle$ and it can be expected that the actual result should belong to this interval. Other measurements are scattered throughout the domain, with four of them clustered in $\langle 4.5, 5.5 \rangle$, which could be a result of a systematic error that occurred occasionally during the measurements. The domain of the data can be divided with the *indexing function* $\tilde{i}(x)$ into intervals, and two divisions are shown: into 20 intervals with the function $\tilde{i}_{20}(x)$ and into 5 intervals with $\tilde{i}_5(x)$.

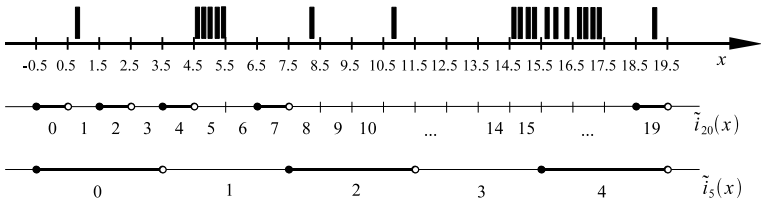

Fig. 2 Data for the illustration of the crisp and fuzzy histogram (up) and data domain intervals: 20 (middle) and 5 (down). All the intervals are left closed and right open, as schematically marked in some of them

The *histogram* of the measurements $\bar{x}^k$ indexed with one of the indexing functions is

$$h_j^l = \sum_{k=1}^{K} \chi[j - \tilde{i}_l(\bar{x}^k)] \tag{1}$$

where $\chi(\cdot)$ is the *characteristic function*

$$\chi(i) = \begin{cases} 1 & \text{if} \quad i = 0 \\ 0 & \text{otherwise} \end{cases} \tag{2}$$

The two histograms obtained with the two indexing functions mentioned are shown in Fig. 3. It can be noted that the mode of neither the histograms reveals the correct estimate of the measured value: in the more accurate one the correct mode has been missed due to an excessive division of the domain, while in the coarser one the accuracy is too low.

The question of the accuracy of indexing in the histogram used as an experimental probability density of a variable in relation to the Hough transform has been treated in many ways. Inhomogeneous, multiresolution and adaptation division were proposed in [7, 14, 21, 27]. Voting distributed among many histogram elements has been proposed in [26]. Fuzzy sets have been applied and the fuzzy Hough transform has been directly introduced in [9]. The

paper by Strauss [24] seems to be the most extensive work on fuzzy histograms in the Hough transform. Not only the problem of uncertainty-precision duality, but also the image thresholding, parameter space quantization, data localization uncertainty, and peak detection in the parameter space, have all been considered.

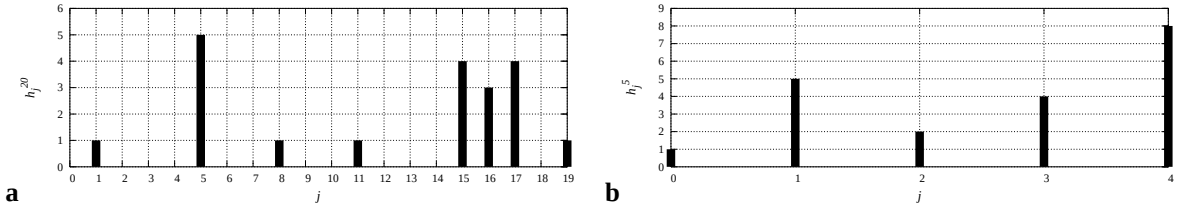

Fig. 3 Histograms of the data of Fig. 2 as obtained with the indexing functions dividing the domain into (a) 20 intervals: h_j^{20}; (b) 5 intervals: h_j^5

The problem of the domain quantization is the problem of *scale*: at which scale the results should be observed? In this presentation, following [2, 3], we shall approach this problem from the point of view of the evidence accumulation in fuzzy histograms, and the problem of scale will be replaced by the question of the upper limit for the fuzzification. Let us define the *fuzzy histogram* (index l of the indexing function is dropped; I is the maximum index in the crisp histogram)

$$h_j^l = \sum_{k=1}^{K} \mu[j - \tilde{\imath}(x^k)] = \sum_{i=0}^{I} \mu(j-i)\, h_i^l \tag{3}$$

where $\mu(\cdot)$ is a fuzzy membership function called in this case the *fuzzification function*.

Coming back to the example, let us define an instance of a fuzzification function using a Gaussian function

$$\mu_G(i) = \begin{cases} e^{-\frac{i^2}{2\sigma^2}} & \text{if } i \in \langle -3\sigma, 3\sigma \rangle \\ 0 & \text{otherwise} \end{cases} \tag{4}$$

Here, σ is the *scale* parameter which controls the range at which the elements of the crisp histogram interact while forming the fuzzy histogram, according to the rightmost part of (3). Let us now observe the evolution of the histogram of Fig. 2 with the changes of the scale, as shown in Fig. 4. As the scale increases, the mode first jumps to the range identified previously as the correct value of the estimate of the measured value at 16. This takes place for a range of small scales, but large enough to allow for the interaction of the neighbouring histogram elements in the fuzzification process. Then, the mode tends to the mean found from the crisp histogram. There exists a limit value at which the mode becomes equal to the mean and further fuzzification makes no change as far as the mode is considered. The fuzzification at this limit will be called the *limit fuzzification*, and the corresponding scale will be called the *limit scale* and will be denoted by $s_{\max}$. Now, the notion of the *fuzzification degree* can be introduced

$$d_f = \frac{s}{s_{\max}} \tag{5}$$

This degree belonging to the range $\langle 0, 1\rangle$ makes it possible to qualify the fuzzification as *weak* when $d_f \approx 0$ and *strong* when $d_f \approx 1$. The question of which scale should be used for fuzzification to receive a good estimate of the quantity accumulated in the histogram as the histogram mode has a simple answer now: *weak fuzzification* should be used.

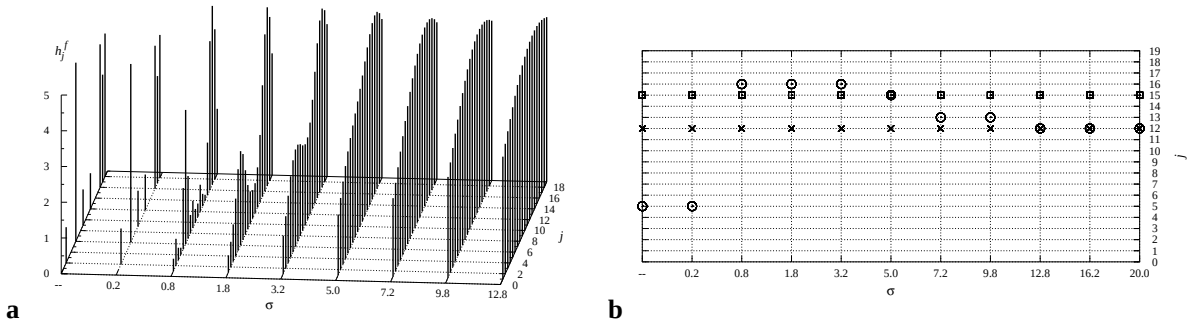

Fig. 4 Changes of the histogram of Fig. 3a fuzzified with the function (4) with changing scale σ. (a) perspective view of the histogram shape; (b) evolution of the mode of the fuzzy histogram (circles) in comparison to the median (squares) and mean (crosses) calculated from the crisp histogram. No fuzzification marked with dashes

The degree of fuzzification can be easily found due to that it is easy to find the limit scale for selected fuzzification functions. In the case of a non-periodic histogram and a clipped quadratic fuzzification function

$$\mu_2(x) = \begin{cases} 1 - \frac{x^2}{s^2} & \text{if } s \neq 0 \text{ and } x \in \langle -s, s\rangle \\ 0 & \text{if } x \notin \langle -s, s\rangle \\ 1 & \text{if } s = 0 \text{ and } x = 0 \end{cases} \tag{6}$$

the limit scale is $s = s_{\max} = i_{\max} - i_{\min}$, that is, the width of the support of the histogram. In other words, the half-width of the fuzzification function equals the width of the histogram support. In the case of a periodic histogram and a clipped cosine square fuzzification function

$$\mu_c(\phi) = \begin{cases} \cos^2 \frac{\pi\phi}{2s} & \text{if } s \neq 0 \text{ and } \phi \in \langle -s, s\rangle \\ 0 & \text{if } \phi \notin \langle -s, s\rangle \\ 1 & \text{if } s = 0 \text{ and } \phi = 0 \end{cases} \tag{7}$$

the limit scale is $s = s_{\max} = T/2$, where T is the period of the histogram. In other words, the width of the fuzzification function equals to the period of the histogram. Simple proofs of these properties can be found in [2, 3]. It is also proved that any real, symmetrical and non-negative function in the form $\mu(x) = f(x/s)$, having a single maximum equal 1 at $x = 0$, has similar properties providing that it is continuous up to the fourth derivative.

The methods presented here are related to robust statistics and to kernel density estimation by the type of functions used as fuzzy membership functions in histogram

fuzzification. The *clipped square* function used in the fuzzification of a non-periodic histogram is related to the *skipped mean* function on the grounds of robust statistics ([12], and later [8, 23]). On the grounds of kernel density estimation, this function is the kernel function derived from the Epanechnikov kernel ([22], as cited by [19], where a broad overview of the applications of robust methods in computer vision problems can be found). The fact that in the case of periodic histograms, the function which has the analogous property is the *clipped cosine square* function has been shown in [2, 3].

2.3. THE ACCUMULATION PRINCIPLE

As stated above, in the image processing problems it is usually recommended to accumulate the information from as many measurements (voting subsets) as possible. This recommendation can be stated as the evidence accumulation principle:

Accumulate the relevant data from possibly many, possibly competent sources.

The accumulation is performed in a histogram. The principle is accompanied by an assumption that quantitatively dominating results are true, which conforms to that the accumulator represents the experimental density of probability of the phenomenon of interest.

The accumulation principle, which has been the basis for the Hough transform and the related methods, expresses a recommendation to use the data redundancy present in images in a specific way. Removing this redundancy early in the processing is possible only in rare cases when the image quality is very high.

3. A TRAINING EXAMPLE: EDGE DETECTION

3.1. PROBLEM FORMULATION

Let us look how a selected problem can be solved with the use of the accumulation principle. The simple problem of edge detection will be considered. We shall not try to construct a new edge detector, but rather to illustrate the way of thinking.

The edge in the image is the locus of pixels in which a significant change of image intensity occurs, so numerical approximations of the differentiating operator are typically used (see for example [1], sect. 3.3). Basically, the intensity values in a pixel and its two neighbours are enough to find the gradient, as shown in Fig. 5a, so the voting subset contains three pixels. The simple equations are as follows

$$\begin{aligned} G_x &= I(1,0) - I(0,0) \\ G_y &= I(0,1) - I(0,0) \\ E &= \left|\vec{G}\right| = \sqrt{G_x^2 + G_y^2} \end{aligned} \tag{8}$$

More combinations of pixels can be used to form coordinate systems in which the gradient can be found. Eight systems possible to form in the first-order neighbourhood of the central pixel are show in Fig. 5b. Other systems can be formed in a systematic way in the higher-order neighbourhoods, as shown in Fig. 6. The gradient, and hence the edge intensity can be found in each of these coordinate systems and transformed to the global system with

the commonly known formulae. For the 2nd order neighbourhood there are 12 measurements, for the 3rd order one – 16 measurements, 4th – 20, 5th – 28, and so on.

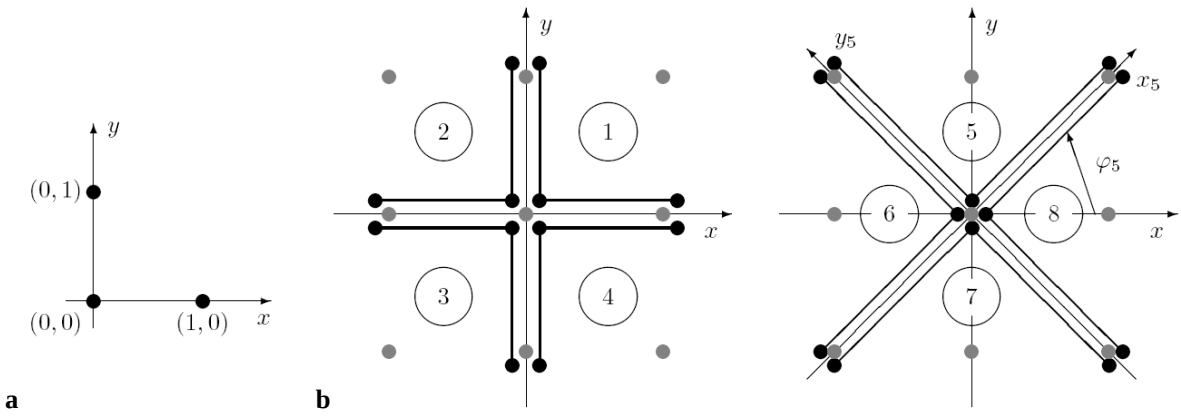

Fig. 5 (a) Basic coordinate system for finding the intensity gradient from three pixels; (b) eight possible coordinate systems in the 1st order neighbourhood of a pixel. Grey points: image pixels; black points and thick lines: axes of local coordinate systems (slightly expanded for visibility), marked with numbers in circles. Angle φ_5 is the angle of rotation of the fifth system with respect to the global system Oxy

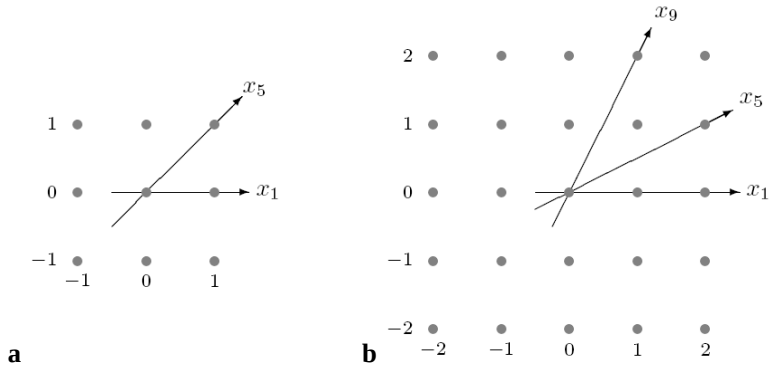

Fig. 6 Forming the coordinate systems in a given pixel (0,0) using its neighbourhoods: (a) 1st order – pixels at distances from 0.5 to 1.5; (b) 2nd order – distances from 1.5 to 2.5. Only the Ox axes determined by the given neighbour for the first one of four systems defined by this pixel are marked; the following three systems emerge by rotating this first one by $\pi/2$, π and $3\pi/2$

From multiple measurements of the gradient, and thus the edge intensity, we now have to obtain a single value. This can be done in several ways. One of them will be the accumulation method, that is, accumulating the measurements in a histogram. This method will be compared here with the finding of the mean value (average) and the median value. The analysis will be restricted to the eight measurements in the 1st order neighbourhood.

3.2. AVERAGE – THE SOBEL DETECTOR

In this case, closed formulae for the gradient components can be found. Laborious but simple calculation reveal that

$$\begin{aligned} G_x &= I(1,1) + 2I(1,0) + I(1,-1) - I(-1,1) - 2I(-1,0) - I(-1,-1) \\ G_y &= I(1,1) + 2I(0,1) + I(-1,1) - I(1,-1) - 2I(0,-1) - I(-1,-1) \end{aligned} \tag{9}$$

It can be seen that these are the formulae of the commonly known and widely and successfully applied Sobel edge detector (e.g. [1], sect. 3.3).

3.3. MEDIAN – THE MEDIAN DETECTOR

The vector median for n vectors is defined as ([18])

$$\vec{v}_m = \arg\min_{i=1}^{n} \sum_{j=1}^{n} d(\vec{v}_i, \vec{v}_j) \tag{10}$$

where $d(\vec{v}_i, \vec{v}_j)$ is the distance between the vectors, and here a simple Euclidean distance was used. In other words, the median is this vector, which has the minimum average distance to all the vectors.

3.4. MODE – THE ACCUMULATION DETECTOR

To accumulate the vectors, a 2-dimensional histogram with the resolution of eight elements for a unit of the gradient was formed. To enhance the results, this histogram was weakly fuzzified with the 2-dimensional version of the function (6). The fuzzification degree $d_f = 0.25$ was taken, and the limit scale was found experimentally to be 108 in the example image. Indeed, the results of the accumulation detector at the limit fuzzification have been exactly the same as those of the Sobel detector. For details please refer to [2].

3.5. EXAMPLE OF RESULTS AND DISCUSSION

Examples of results obtained with the three detectors for the test image already shown in Fig. 1a, for which the graph of the image intensity is shown in Fig. 7a, have been shown in Fig. 7b, c and d.

The results show that the averaging, Sobel detector performs the best for the given image. The fact that the accumulation detector attains the quality of the averaging detector only at the limit fuzzification means that the number of measurements taken into account was too small to have statistically meaningful results. The considerations presented in this Section remain only an exercise in the design of an accumulation method in a simple image processing problem. An interesting side-effect of this exercise is that the known Sobel detector is a member of the same family of the detectors based on the eight gradient measurements in the 1st order neighbourhood of the pixel, to which the considered accumulation detector belongs, and that this Sobel detector can be considered as the limit case of the accumulation detector at the limit fuzzification.

It should be added in the end that the image shown previously in Fig. 1b has been obtained with the basic detector described by (8), and that of Fig. 1c has been found with the further enhanced version of the accumulation detector considered above. The enhancement consisted in that the results were fuzzified along the edge direction, found as the direction normal to the local gradient, with the cosine square membership function according to (7) having the support of 16 pixels, centred at the pixel considered.

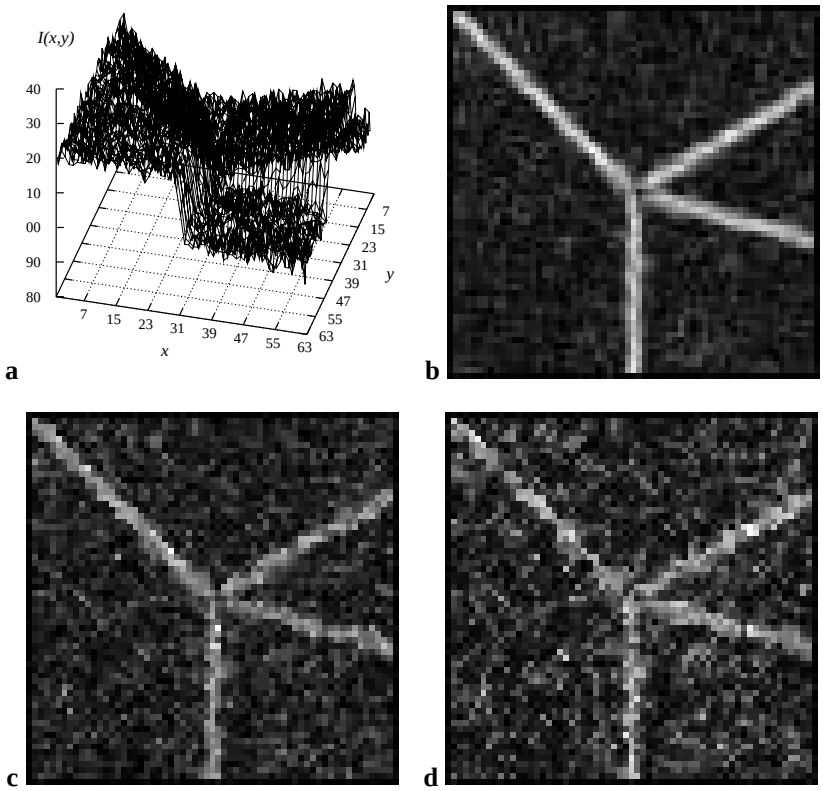

Fig. 7 Results of edge detection with the three detectors considered for the test image of Fig. 1a. (a) Graph of the intensity function of the test image; (b) result of the averaging, Sobel detector; (c) result of the median detector; (d) result of the accumulation detector

4. VERIFYING THE WEAK FUZZIFICATION: IMAGE REGISTRATION

The weak fuzzification as a recommendation in the case of difficult data has been verified in test problems of image registration with high share of noise in the data. These examples have been thoroughly described in [2] and to some extent in [3]. Here, one of them will be recapitulated.

The test image is the *simulation image* made routinely during the preparation of the treatment of cancer by irradiation with external beams (see [2, 3] for references). In this image some edges of bony structures have been selected for registration. The reference and the overlaid image have been obtained by translation and rotation of these selected pixels, as shown and specified in Fig. 8. The data have been contaminated by randomly selecting a part ζ of the pixels, separately in both images, and moving each of them into a different position selected at random from the whole image with uniform probability. In this way each of the images contained ζ outliers and $1-\zeta$ inliers. A set of image pairs with ζ varying from 0.0 to 0.9 has been formed.

If the rigid transformation is used for registration, the voting subset contains two pixels (a line segment) from each of the images, which makes it possible to find the three transformation parameters: two translation components and a rotation angle (with no scaling, the set of possible line segments is limited to those of equal length). Hundreds of thousands

voting subsets were accumulated. The $81\times81\times201$ accumulator array allowed for translation of ±20 pixels in each direction and rotation of $\pm20^{o}$, and was fuzzified with a 3-dimensional version of the square fuzzification function (6). Calculations were performed for each share of outliers ζ and 12 values of the fuzzification degree. The received registration error, calculated as the maximum distance of an overlaid pixel from the set of reference pixels, found for undistorted images, has been plotted in Fig. 9.

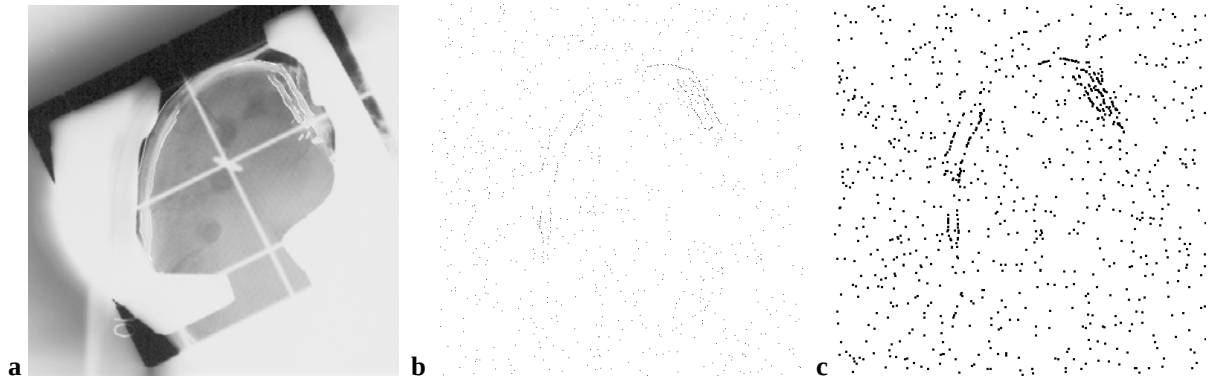

Fig. 8 Example images 500×500 for the image registration test. (a) Source image – edges of bony structures selected for registration marked with white pixels; (b) reference image received from image a by translating the selected edges 3 pixels left, 2 pixels down and rotating by 4°; (c) overlaid image received from a by rotating by -1°, enhanced for visualisation by replacing each pixel with 4 pixels. Images b, c contain $\zeta=0.8$ of outliers

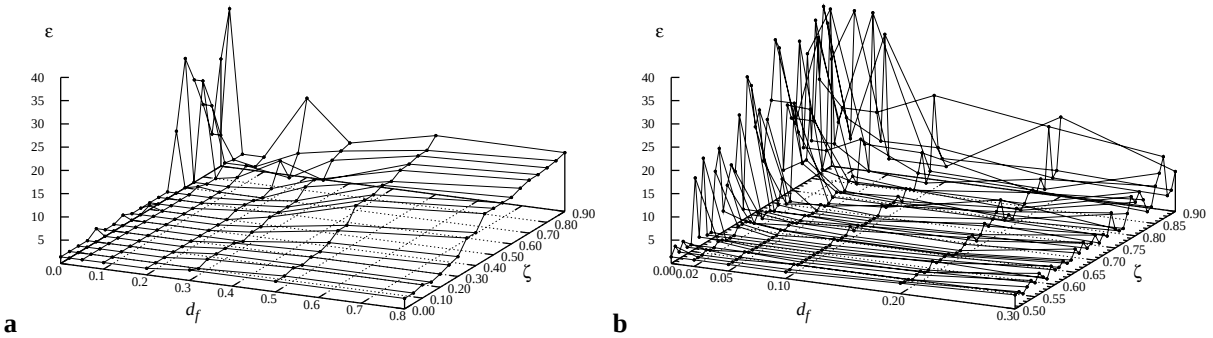

Fig. 9 Registration error for imges of Fig. 8b, c. (a) coarse, large-scale graph; (b) small-scale graph for small d_f

It can be seen in the graphs that for no fuzzification the registration errors are large for $\zeta>0.5$ of outliers in the data. For weak fuzzification at $d_f\in\langle0.05,0.20\rangle$ the errors are acceptably small (here, 5 pixels error can be accepted) up to the share around 0.8 of data.

This observation can be considered as the confirmation of the recommendation of weak fuzzification, at $d_f\in\langle0.05,0.20\rangle$, in the given example.

5. USING THE ACCUMULATION PRINCIPLE: LINE DETECTION

The accumulation principle and the recommendation of weak fuzzification has been used to propose a new detector of quasi-linear structures in the images, described successively in [2, 3, 4, 5, 6]. This detector has been designed mainly, but not exclusively, for biomedical

applications due to it good properties in noisy images and good invariance to direction and line width. An example of a mammographic image fragment is shown in Fig. 10.

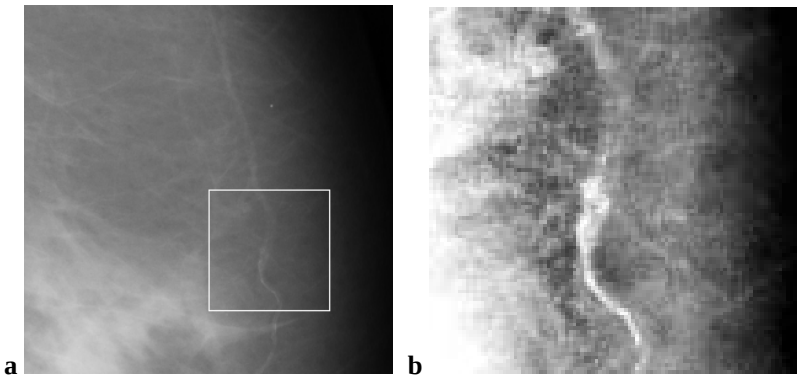

Fig. 10 Example image for line detection: fragment of image `mdb042` from the mini-MIAS database of mammograms [25]. (a) larger fragment; (b) fragment 100×100 for tests (enhanced for visualization)

The voting subset is now a pair of pixels p_1, p_2 as shown in Fig. 11. The image gradients $\vec{G}_1, \vec{G}_2$ are rotated by $\pi/2$ in opposite directions to form tangent vectors $\vec{\vec{T}}_1, \vec{\vec{T}}_2$ that are summed to form the vector $\vec{V}$. The direction and modulus of this vector makes it possible to calculate the line direction and width (see Fig. 11) and intensity in the central pixel p_c of the voting pair. The final line intensity accumulated throughout the image from all the possible voting pairs (fulfilling a set of commonsense geometrical conditions, like that the gradients should not be directed outwards the voting pair) used in voting in all the image pixels is found as

$$l = c_d c_e \left|\vec{V}\right| / w \tag{11}$$

Where $c_d \in \langle 0,1 \rangle$ is the directional consistence coefficient equal one when tangent vectors are parallel, and $c_e \in \langle 0,1 \rangle$ is the coefficient of edgeness consistence equal one when moduli of gradients are equal. In the accumulation, the line intensity is treated as a periodic value with respect to the line direction, with the period π. Detailed formulae and discussion of eq. (11) can be found in [2]. Effectively, several hundreds of voting subsets, belonging to a large area around each pixel (Fig. 11b), have been voting for line intensity at each pixel, so the negative effects of a small number of votes, visible in the accumulation edge detector in Section 3, could not occur here. The accumulator conforming to the image space is three-dimensional: two image dimensions and line width (within a pre-specified range). Several fuzzifications are performed in the accumulator: limit fuzzification along the angle – for reducing the accumulator dimensionality from 4 to 3; weak fuzzification of the location of the central pixel – to compensate for non-integer locations of this pixel and to stabilize the results; weak fuzzification along line width – to enhance the detector isotropy; and along the line direction – to enhance the line continuity. After accumulation, local line intensity maxima higher than the line intensity threshold f_l are found, line ridges are sought for from them, and line widths are plotted in the ridges to find the line.

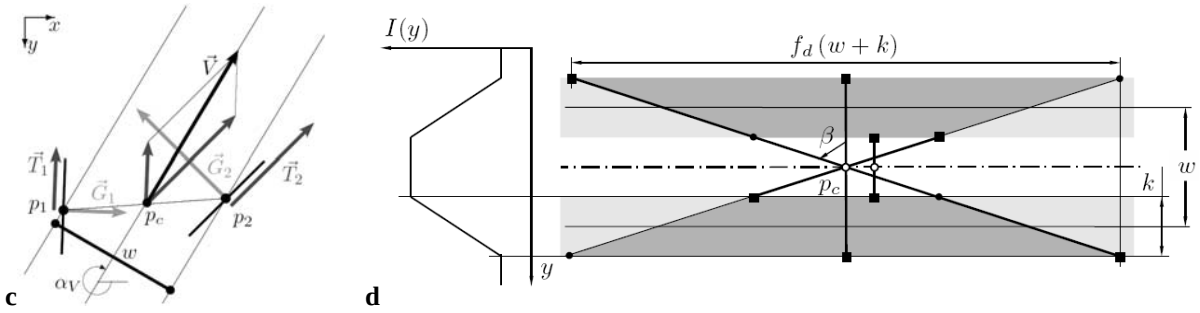

Fig. 11 (a) Geometry of the line model; (b) region of possible voting pixels (dark grey) for an idealized line as in the intensity graph on the left; bright grey: regions of nonzero gradient; points connected with lines: extreme examples of voting pairs; pair with minimum distance (squares) displaced to the right for visibility

Results of line detection for the image of Fig. 10b have been shown in Fig. 12. Line continuity has been maintained besides that its contrast is strongly varying along it.

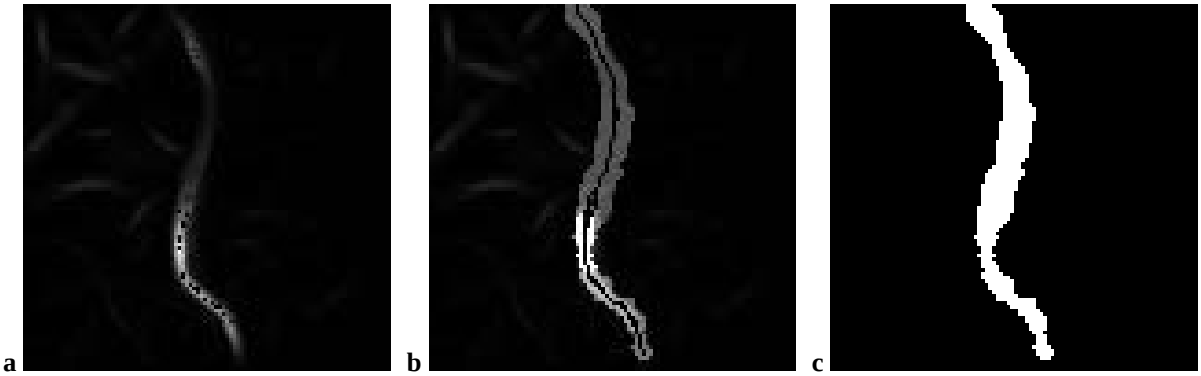

Fig. 12 Results of line detection in the image of Fig. 10. (a) Maximum line intensity across line widths with local maxima (black); (b) ridge pixels sought for from the maxima (black) and line widths marked with the same intensities as in corresponding ridge pixels; (c) binary mask of the line – all width pixels set to white

To check the properties and limits of the detector presented above, several series of tests have been performed [2]. Here, the testing for robustness to noise will be briefed. An artificial test image shown in Fig. 13a and d has been used. This image has three levels of grey, close to each other: 100 (background), 110 (thin lines) and 115 (thick lines). A series of such images has been formed, noiseless and with centred normal noise of seven standard deviations from 1.92 to 15.29, which has formed a series of images with the signal to noise ratio of ∞, 9, 6, …, -6, -9 dB. Detection results were compared to the ideal ones and ROC curves for each SNR were plotted, using the line intensity threshold f_l as the cutoff parameter [20]. The ROC curve for the largest noise for which the result were still very acceptable, that is, SNR=-3 dB, has been shown in Fig. 13c. The method breaks down totally for SNR between -6 dB and -9 db.

To see how the noise at SNR=-3 dB relates to the noise present in a typical mammogram, the graphs of the image intensity of the fragment of the image of Fig. 13a and the image of Fig. 10b have been plotted alongside in Fig. 13d and e. The examination of these images reveals that a typical mammogram should have the noise at the level at most not larger than that of Fig. 13a, that is, at SNR<-3 db. This can be treated as an indication that the robustness of the detector presented against noise is good enough for the analysis of mammographic images.

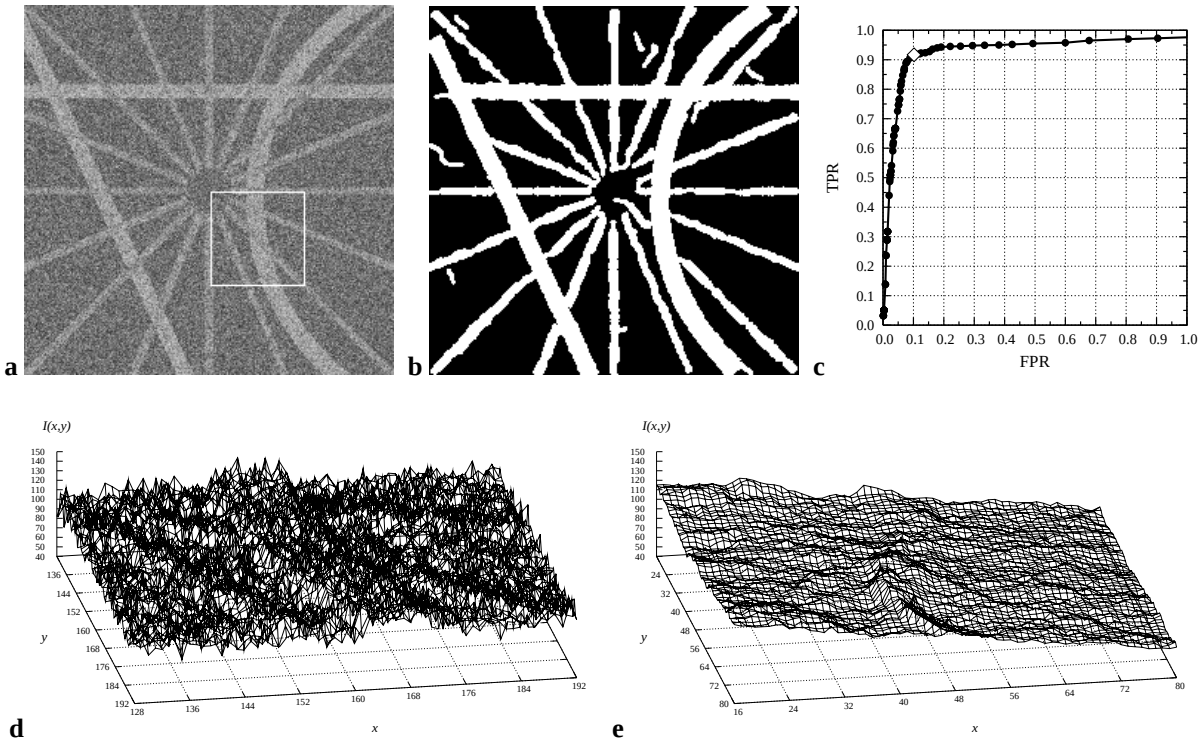

Fig. 13 (a) Test image 250×250; here the realization with noise at SNR=-3 dB is shown (contrast enhanced for better visualization); (b) result of line detection for image a; (c) ROC curve at the same SNR with the working point at TPR=0.917, FPR=0.011, marked with a rhombus; (d), (e) graphs of image intensity of the fragment of the image a (marked there with a square), and the image of Fig. 10b, both in the same scale

6. CONSLUSION

The accumulation principle, used in the past in the methods related to the HT, and the recommendation to use weak fuzzification, as defined in the previous publications, make it possible to design the image processing methods which are robust against strong noise, even the noise having the level exceeding the level of the signal in the image. The proper organization of the accumulation process, with sufficiently large numbers of voting subsets, makes it possible to solve specified image analysis tasks for difficult images. The accumulation in image space makes it possible to find quasi-linear object having the shape which can not be parameterized.

In the training example of an accumulation method for edge detection it has been discovered that the known Sobel edge detector belongs to the same family of detectors as the corresponding accumulation-type detector in the first-order neighbourhood of a pixel. The Sobel detector can be treated as the limit case of an accumulation detector, at the limit fuzzification. The accumulation methods are a good solution to the problem of analysis of such images.

BIBLIOGRAPHY

[1] BALLARD D.H., Brown C.M., Computer vision, Prentice Hall, Englewood Cliffs, 1982.
[2] CHMIELEWSKI L.J., Metody akumulacji danych w analizie obrazów cyfrowych (Evidence accumulation methods in digital image processing). Akademicka Oficyna Wydawnicza EXIT, Warsaw, 2006. http://akum06.xt.pl .

[3] CHMIELEWSKI L.J., Fuzzy histograms, weak fuzzification and accumulation of periodic quantities. Application in two accumulation-based image processing methods, Pattern Analysis and Applications, Vol. 9, No. 2-3, 2006.
[4] CHMIELEWSKI L., Specification of the evidence accumulation-based line detection algorithm, Advances in Soft Computing, Vol. 30, pp 355-362, 2005.
[5] CHMIELEWSKI L., Scale and direction invariance of the evidence of the accumulation-based line detection algorithm, Advances in Soft Computing, Vol. 30, pp 363-370, 2005.
[6] CHMIELEWSKI L., Detection of non-parametric lines by evidence accumulation: Finding blood vessels in mammograms, Computational Imaging and Vision, Vol. 32, pp 373-380, 2004.
[7] COHEN M., TOUSSAINT G., On the detection of structures in noisy pictures. Pattern Recognition, Vol. 9, pp. 95-98, 1977.
[8] HAMPEL F.R., RONCHETII E.M., ROUSSEEUW P.J., STAHEL W.A., Robust statistics: the approach based on influence functions, John Wiley, New York, 1986.
[9] HAN J.H., KÓCZY L.T., POSTON T., Fuzzy Hough transform, Pattern Recognition Letters, Vol. 15, No. 7, pp. 649-658, 1994.
[10] HOUGH P.V.C., A method and means for recognizing complex patterns, U.S. Patent 3.069.654, Dec 18, 1962.
[11] HOUGH P.V.C., Machine analysis of bubble chamber pictures, Proc. Int. Conf. on High Energy Accelerators and Instrumentation, CERN, 1959.
[12] HUBER P.J., Robust Statistics, John Wiley, New York, 2003.
[13] ILLINGWORTH J., KITTLER J., A survey of the Hough transform, Comp. Vision, Graph., and Image Proc., Vol. 44, No. 1, pp. 87-116, 1988.
[14] JOLION J., ROZENFELD A., A 0 log *n* pyramid Hough transform, Pattern Recognition Letters, Vol. 9, pp. 343-349, 1989.
[15] KÄLVIÄINEN H., HIRVONEN P., ERKKI O., Probabilistic and non-probabilistic Hough transforms: overview and comparisons. Image and Vision Computing, Vol. 13, No. 4, pp. 239-252, 1995.
[16] KULCZYCKI P., Estymatory jądrowe w analizie systemowej (Kernel estimators in systems analysis), Wydawnictwa Naukowo-Techniczne, Warszawa, 2005.
[17] LEAVERS V.F., Which Hough transform?, CVGIP: Image Understanding, Vol. 58, pp. 250-264, 1993.
[18] LUKAC R., PLATANIOTIS K.N., VENETSANOPOULOS A.N., SMOLKA B., A statistically-switched adaptive vector median filter, J. Intelligent and Robotic Systems, Vol. 42, No. 4, pp. 361-391, 2005.
[19] MEER P., Robust techniques for computer vision, In MEDIONI G., Kang S.B., Editors, Emerging topics in computer vision, pp. 107-190. Prentice Hall, 2004.
[20] OBUCHOWSKI N.A., Receiver operating characteristic curves and their use in radiology, Radiology, Vol. 229, No. 1, pp. 3-8, 2003.
[21] O'ROURKE J., SLOAN K., Dynamic quantization: Two adaptive data structures for multidimensional space. IEEE Trans. PAMI, Vol. 3, pp. 266-288, 1984.
[22] PARZEN E., On estimation of a probability density function and mode, Ann. Math. Statist., Vol. 33, pp. 1065-1076, 1962.
[23] ROUSSEEUW P.J., LEROY A.M., Robust Regression and Outlier Detection, John Wiley, 1987.
[24] STRAUSS O., Use the Fuzzy Hough Transform towards reduction of the precision-uncertainty duality, Pattern Recognition, Vol. 32, pp. 1911-1922, 1999.
[25] SUCKLING J., PARKER J. et al., The Mammographic Images Analysis Society digital mammogram database, in GALE A.G., ASTLEY S.M. et al., Eds., Digital Mammography, Exerpta Medica International Congress Series, Vol. 1069, Elsevier, pp. 375-378, 1994. http://peipa.essex.ac.uk/info/mias.html .
[26] THRIFT P., DUNN S., Approximating point-set images by line segments using a variance of the Hough transform, Comp. Vision, Graph., and Image Proc., Vol. 21, pp. 383-394, 1983.
[27] Van VEEN T., GRŒN F., Discretization errors in the Hough transform, Pattern Recognition, Vol. 14, pp. 137-145, 1981.